AMERICAN SOCIETY FOR MICROBIOLOGY | mSystems®

RESEARCH ARTICLE
Host-Microbe Biology

Multiplexed Competition in a Synthetic Squid Light Organ Microbiome Using Barcode-Tagged Gene Deletions

Hector L. Burgos,[a] Emanuel F. Burgos,[a] Andrew J. Steinberger,[b] Garret Suen,[b] Mark J. Mandel[a]

[a]Department of Medical Microbiology and Immunology, University of Wisconsin—Madison, Madison, Wisconsin, USA
[b]Department of Bacteriology, University of Wisconsin—Madison, Madison, Wisconsin, USA

ABSTRACT Beneficial symbioses between microbes and their eukaryotic hosts are ubiquitous and have widespread impacts on host health and development. The binary symbiosis between the bioluminescent bacterium *Vibrio fischeri* and its squid host *Euprymna scolopes* serves as a model system to study molecular mechanisms at the microbe-animal interface. To identify colonization factors in this system, our lab previously conducted a global transposon insertion sequencing (INSeq) screen and identified over 300 putative novel squid colonization factors in *V. fischeri*. To pursue mechanistic studies on these candidate genes, we present an approach to quickly generate barcode-tagged gene deletions and perform high-throughput squid competition experiments with detection of the proportion of each strain in the mixture by barcode sequencing (BarSeq). Our deletion approach improves on previous techniques based on splicing by overlap extension PCR (SOE-PCR) and *tfoX*-based natural transformation by incorporating a randomized barcode that results in unique DNA sequences within each deletion scar. Amplicon sequencing of the pool of barcoded strains before and after colonization faithfully reports on known colonization factors and provides increased sensitivity over colony counting methods. BarSeq enables rapid and sensitive characterization of the molecular factors involved in establishing the *Vibrio*-squid symbiosis and provides a valuable tool to interrogate the molecular dialogue at microbe-animal host interfaces.

IMPORTANCE Beneficial microbes play essential roles in the health and development of their hosts. However, the complexity of animal microbiomes and general genetic intractability of their symbionts have made it difficult to study the coevolved mechanisms for establishing and maintaining specificity at the microbe-animal host interface. Model symbioses are therefore invaluable for studying the mechanisms of beneficial microbe-host interactions. Here, we present a combined barcode-tagged deletion and BarSeq approach to interrogate the molecular dialogue that ensures specific and reproducible colonization of the Hawaiian bobtail squid by *Vibrio fischeri*. The ability to precisely manipulate the bacterial genome, combined with multiplex colonization assays, will accelerate the use of this valuable model system for mechanistic studies of how environmental microbes—both beneficial and pathogenic—colonize specific animal hosts.

KEYWORDS barcode sequencing, amplicon sequencing, sequence-tagged gene deletions, *Vibrio fischeri*, *Aliivibrio fischeri*, BarSeq

Beneficial symbioses are ubiquitous in the environment and have substantial impacts on the health and development of animal hosts. In animals, symbionts can affect host organ morphogenesis, immune system development, reproduction, susceptibility to disease, and even behavior (1–4). In humans, the gut, skin, lungs, and urogenital tract all have specific microbiomes for which their dysbiosis has been associated with disease

Citation Burgos HL, Burgos EF, Steinberger AJ, Suen G, Mandel MJ. 2020. Multiplexed competition in a synthetic squid light organ microbiome using barcode-tagged gene deletions. mSystems 5:e00846-20. https://doi.org/10.1128/mSystems.00846-20.

Editor Benjamin E. Wolfe, Tufts University

Address correspondence to Mark J. Mandel, mmandel@wisc.edu.

Received 24 August 2020
Accepted 18 November 2020
Published 15 December 2020

(5–8). It is clear that molecular communication between animal hosts and their microbial partners leads to selection and retention of the cognate microbiome: while many microbes are obtained from the environment, the composition of mature microbiomes is often largely stable and resilient within members of a host species (9, 10). While microbial communities have been characterized using metagenomic, transcriptomic, and metabolomic approaches (11), the complexity of animal-associated microbiomes and the inability to culture and genetically manipulate many symbionts make it difficult to study the precise molecular mechanisms that establish specific relationships.

The binary symbiosis between genetically tractable *Vibrio fischeri* and the Hawaiian bobtail squid *Euprymna scolopes* serves as a model system to study the molecular interactions underlying microbiome assembly (11–16). The squid hatch aposymbiotically (without symbiont) and are colonized by *V. fischeri* in a multistep process that leads to the specific recruitment of the symbiont from a marine environment in which the bacteria are $<$0.1% of the bacterioplankton (14, 17). The symbionts are housed in the dedicated light organ (LO) within the squid's mantle cavity, where they generate light that the host uses for counterillumination to hide its shadow while hunting at night (18). The host provides the symbionts with a protected niche, nutrients, and oxygen (15). Once the symbiosis is irreversibly established in juvenile squid, a daily cycle proceeds where 90 to 95% of the bacteria are expelled from the LO at dawn. The remaining symbionts grow during the day until they fill the LO, and at night the dense population of symbionts provides light (19). Because the aposymbiotic hatchlings can be cultured in the lab and infected with genetically tractable *V. fischeri*, colonization experiments can be performed to study the molecular factors that play a role during this process (12, 16, 20). In addition, the translucent nature of the LO in squid hatchlings allows for visualization of the colonization process by microscopy (21–23).

Microbe-host signaling mechanisms and developmental transitions ensure specificity during colonization (14, 17). Upon detection of bacterium-derived peptidoglycan, the ciliated appendages on the surface of the LO secrete mucus that traps bacteria circulating within the mantle cavity (13, 24, 25). In the mucus field, *V. fischeri* bacteria bind to cilia and form aggregates by expressing symbiosis polysaccharide (*syp*) genes, a locus of 18 structural and regulatory genes whose products contribute to biofilm formation (26, 27). Approximately 3 to 4 h postinoculation, bacterial aggregates migrate through the host mucus toward the pores that lead into the LO ducts (25). While the initial migration is independent of flagellar motility (28), at the pores squid-produced chitin oligosaccharides serve as a chemoattractant to direct the symbiotic bacteria into the host crypts (21). Motility and chemotaxis are required for colonization, and strains with mutations in genes required for these processes—such as *cheA*, *flrA*, and *rpoN*—are unable to successfully colonize the squid LO (21, 28). Once within the LO *V. fischeri* generates light through expression of the *lux* operon in a quorum sensing-dependent process (29). Symbionts that fail to produce luminescence, such as strains with mutations in the autoinducer synthase genes *ainS* and *luxI*, or deletions of the *lux* operon, are unable to persist in the symbiosis (30, 31).

To identify novel colonization factors in *V. fischeri*, our lab previously used a global transposon insertion sequencing approach (INSeq) to identify bacterial mutants that were depleted after 48 h in the squid host (32). This approach successfully identified previously known colonization factors, such as *rscS*, *rpoN*, *ompU*, various motility factors, and the *syp* biofilm locus, and in addition revealed 344 putative novel colonization factors. Twenty candidates were tested in competitive colonization assays of wild-type (WT) versus mutant strains, and the results showed that nine factors had colonization defects. Some of the validated factors encompass roles in protein quality control (DnaJ and DegS) and copper detoxification (CopA and CusC), inner membrane proteins predicted to play a role in secretion of autotransporters (TamB/YtfN), and other poorly characterized factors (YdhC, YafD, and YhcB). This global approach was crucial in identifying putative colonization factors. However, further study is required

to address which genes are true colonization factors, when they act during colonization, and how their products modulate the interaction with the host.

Approximately 32% of putative colonization factors identified by INSeq did not fall into a curated Clusters of Orthologous Groups (COGs) category, suggesting that the ability to interrogate the function of these colonization factors will reveal novel biology. Traditional genetic engineering techniques in *V. fischeri* are either random (transposon mutagenesis) or labor-intensive (plasmid-based allelic exchange) (32–34). We therefore considered approaches by which we could isolate mutants and examine phenotypes in a multiplexed fashion. One possible approach was to retrieve transposon insertions of interest from an arrayed library (35–37). A second approach we considered was to adapt a newly developed method for transformation-mediated mutagenesis using linear DNA (38) with an in-frame barcoding strategy to facilitate precise mutations. The latter option was attractive in that we hoped that it would limit the effects of polar mutations and provide a set of defined deletions that can be characterized by amplicon PCR. Barcode sequencing (BarSeq), in which each strain is uniquely labeled and identified using high-throughput next-generation sequencing, has been used successfully to track population dynamics in multiple systems, including in yeast genomic libraries, during *Vibrio cholerae* infection, and to track and phenotype laboratory-evolved *Escherichia coli* (39–43). Here, we describe an approach to generate barcode-tagged gene deletions in *V. fischeri* and perform high-throughput colonization experiments using BarSeq. We also describe the barseq python computational package used to analyze the results.

RESULTS

Generation of barcoded gene deletions. To generate barcoded deletions of specific *V. fischeri* genes, we designed an approach that takes advantage of splicing by overlap extension PCR (SOE-PCR) and *tfoX*-based natural transformation (Fig. 1) (38, 44–46). The first step uses PCR to amplify DNA fragments upstream and downstream of the gene targeted for deletion, fused to the left and right linker sequences, respectively (Fig. 1A). A separate PCR is performed with pHB1 as a template to generate the central fragment of DNA containing the linker sequences, a selectable marker (*erm*, conferring erythromycin resistance) surrounded by FLP recombination target (FRT) sites, and the semirandom barcode sequence. The barcode is provided by the reverse primer, which contains a region of semirandomized sequence. The three resulting DNA fragments—upstream, central, and downstream—are then fused into one fragment via their overlapping linker sequences by SOE-PCR (46) and transformed into *V. fischeri* upon *tfoX* induction (44). Finally, the *erm* cassette is removed via FLP recombinase (45).

The resulting 138-bp deletion scar (*barcode* scar, or "*bar*" scar, Fig. 1B) lies between the deleted gene's first codon and last seven codons (i.e., the final six amino acid-encoding codons plus the stop codon). The scar is designed to be in-frame to prevent polar effects on gene expression when targeting genes within operons. The terminal codons were retained in case they contain a ribosomal binding site for downstream gene(s) (47). In addition to the barcode, the additional sequence in the scar includes left and right linker sequences that are shared among all of the mutants, which allows us to identify and quantify the abundance of each barcoded strain using amplicon sequencing, while minimizing amplification bias by using common primers that amplify the same size product.

To test this new approach, we investigated the *copA* gene. Among *Gammaproteobacteria*, CopA is the main exporter of cytoplasmic copper and is the most widely conserved copper detoxification factor (48, 49). Although our laboratory previously demonstrated that *copA* is a squid colonization factor, its role in copper resistance has not been examined (32). We therefore targeted *copA* for deletion using our mutagenesis approach as a proof of concept and subsequently tested its role in copper resistance in *V. fischeri*. To ensure that the deletion process worked as intended, we used four sets of diagnostic PCR primers that would report on correct *erm* insertion, subsequent removal of the *erm* cassette

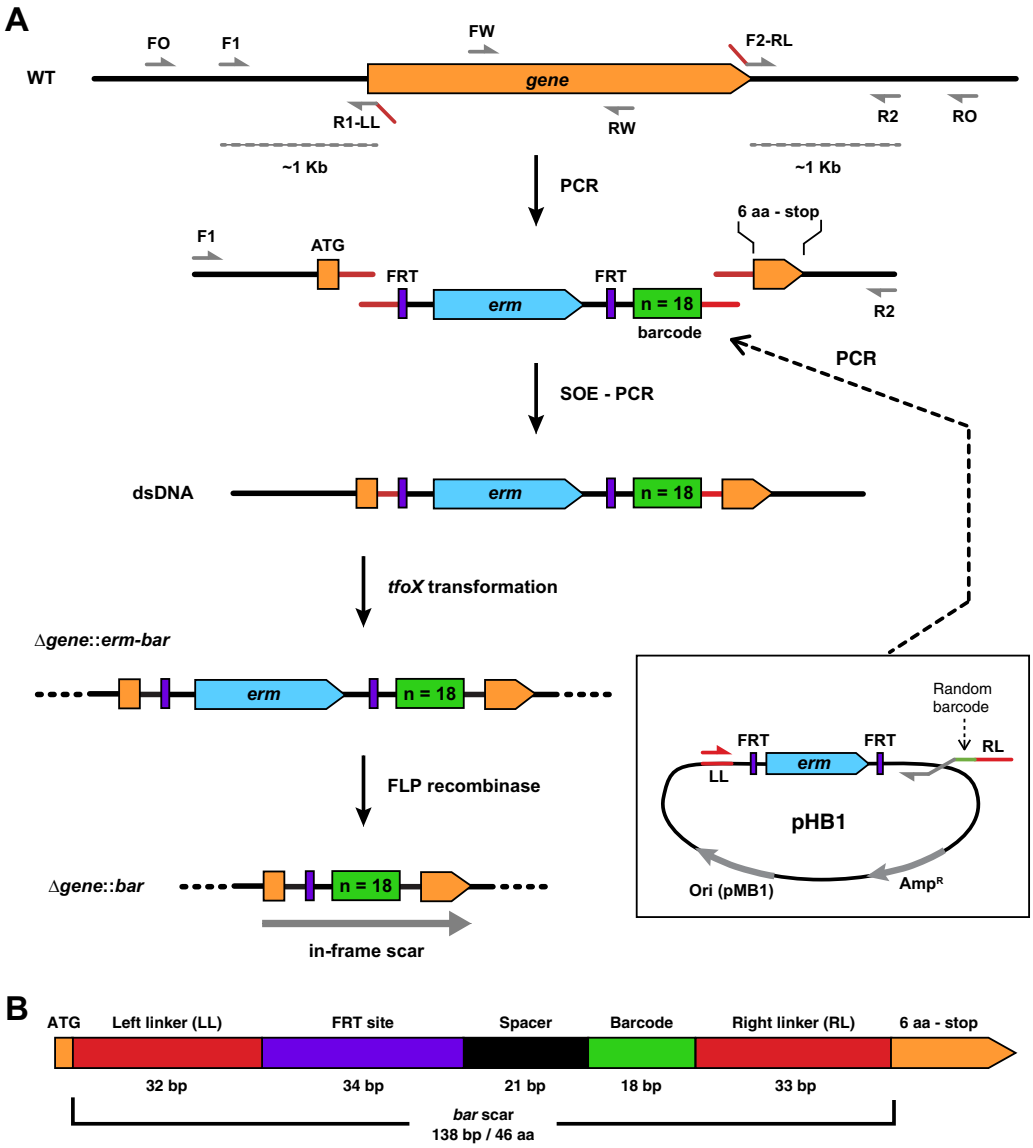

FIG 1 Approach for quickly generating barcode-tagged gene deletions in *V. fischeri*. (A) Schematic diagram (not to scale) of the process used to generate the barcoded deletions as described in the main text. Multiple primers are designed for use in PCR to generate the desired DNA molecules and screen/sequence for the correct deletion mutants as described in Materials and Methods. (B) Schematic of the resulting *bar* scar containing the start codon, the left and right linker sequences (LL and RL), the FRT site that remains after removal of the *erm* cassette, a spacer sequence, the unique barcode, and the last seven codons of the targeted open reading frame (ORF). The schematic is drawn to scale. The barcode sequence is designed to lack in-frame stop codons, which results in an in-frame ORF together with the start codon and the last seven codons of the targeted gene.

by FLP recombinase, and absence of the targeted gene from the bacterial chromosome. PCR with various pairs of oligonucleotides that target the *copA* gene and its deletion constructs produced amplicons of the expected size in each strain (Fig. 2A). These results show that the *erm* cassette was successfully inserted into *copA* generating Δ*copA*::*erm-bar* and subsequently removed by FLP recombination to generate the in-frame deletion scar in Δ*copA*::*bar*. Furthermore, sequencing of the deletion scar for several Δ*copA*::*erm-bar* candidates showed that after a single round of mutagenesis, multiple uniquely barcoded deletion strains were generated (Fig. 2B). These results demonstrate that our deletion method is successful in generating uniquely barcoded mutant strains of *V. fischeri*.

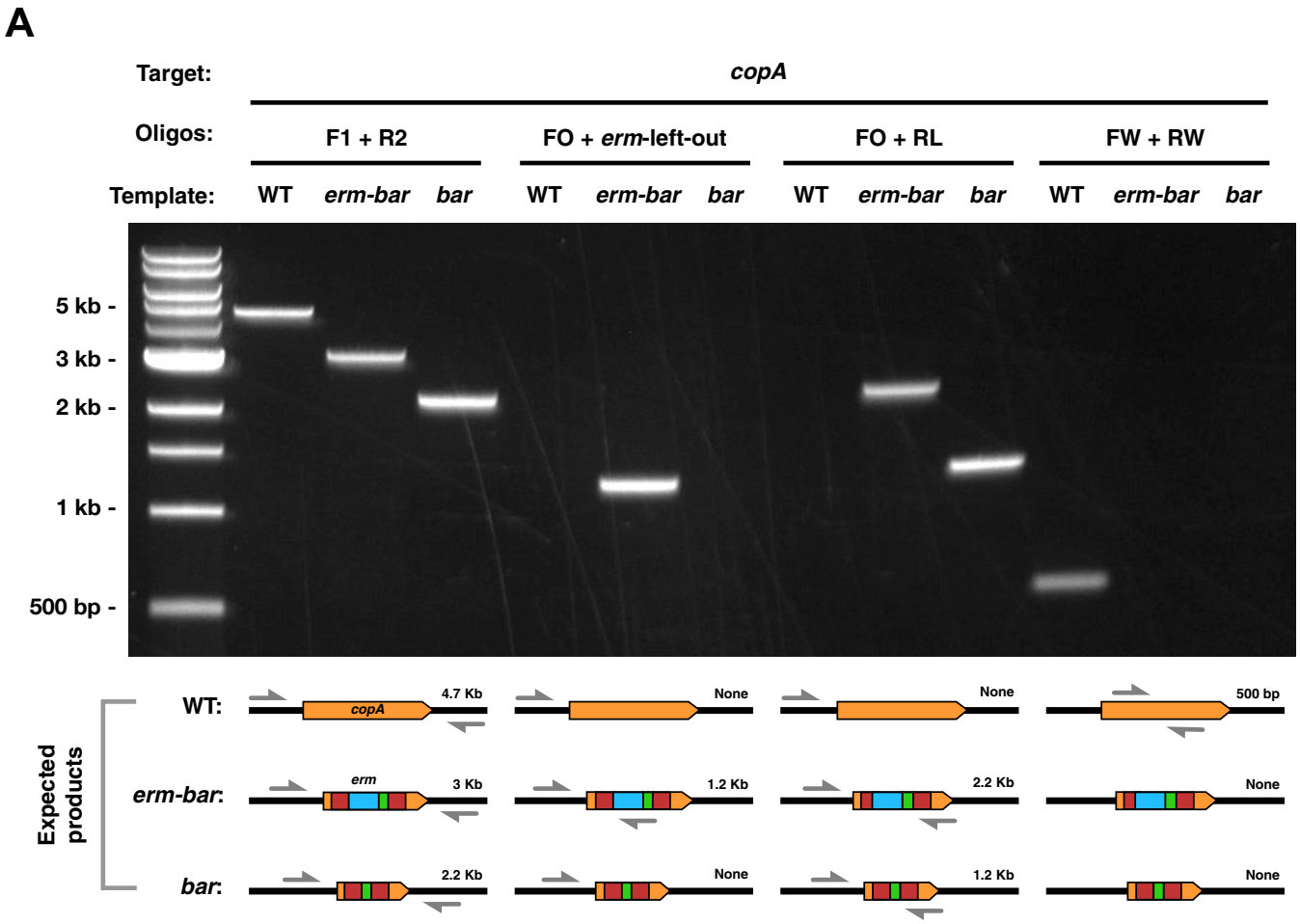

FIG 2 Evaluating the genotype of a *copA* deletion strain. (A) Representative 1% agarose gel showing the products generated by PCR when using the specified primer pairs and templates. DNA ladder is the 1-kb Plus DNA ladder (New England BioLabs). Oligos, oligonucleotides. (B) Table showing several unique barcode sequences within the Δ*copA*::*erm-bar* deletion scar of various deletion candidates that were generated from a single round of mutagenesis. The diagram is not drawn to scale.

The presence of a barcode within a gene deletion does not alter mutant phenotypes. To test that the barcoded scar does not affect the mutant phenotypes, we measured the copper sensitivity of strains deleted for *copA* using various methods. In addition to the mutants generated using our deletion approach (Δ*copA*::*erm-bar* and Δ*copA*::*bar*), we constructed a deletion of *copA* using plasmid-based allelic exchange

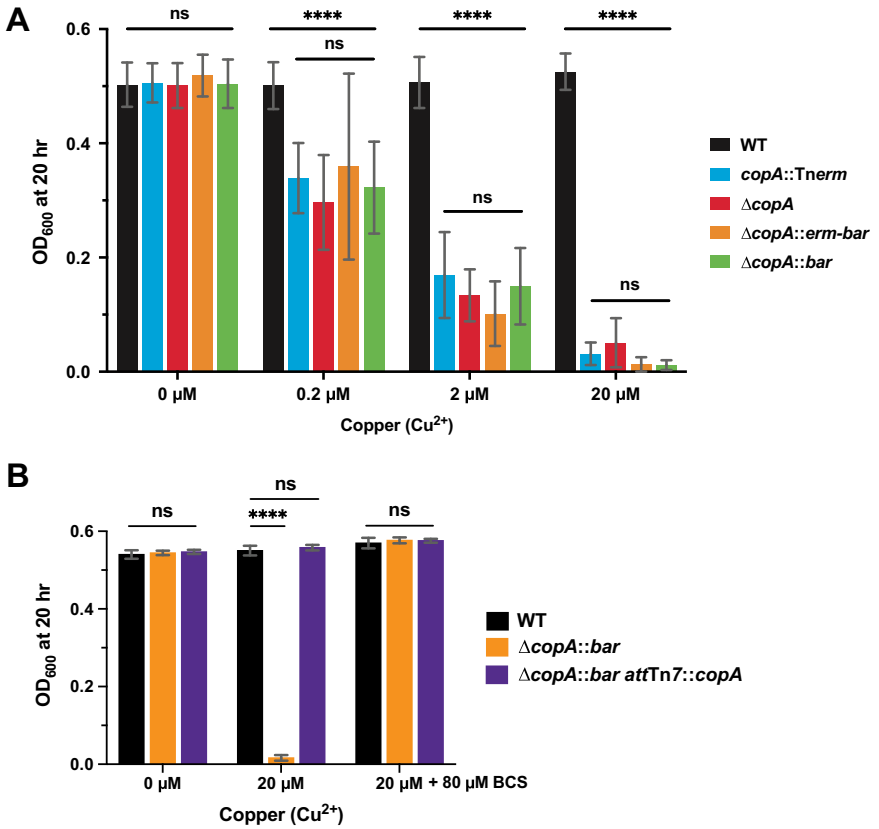

FIG 3 Assaying the phenotype of strains lacking copper resistance factor CopA. (A and B) Bar graphs showing the average OD_{600} of the indicated *copA* mutants after 20 h of growth in the presence of the indicated amounts of copper and/or bathocuproinedisulfonic acid (BCS). (A) Error bars represent the standard deviations of the means ($n = 3$). (B) Data are from two independent replicates ($n = 2$). Statistical analysis was performed using a two-way analysis of variance (ANOVA) test. ****, $P < 0.0001$; ns, not significant.

(Δ*copA*) (33) and obtained a *copA* transposon mutant isolated from our previous study (*copA*::Tn*erm*) (32). We then tested the growth of these *copA* mutants in the presence of various amounts of copper. Our results show that, regardless of the mutagenesis method, the growth of *copA* mutants is similarly impeded in the presence of copper, with the severity of the growth defect increasing in proportion to the concentration of copper: at 0.2 μM Cu^{2+}, the *copA* mutants were able to grow slightly, whereas at 20 μM Cu^{2+}, these strains were unable to grow (Fig. 3A). This is in contrast to the WT strain that achieved the same growth yield regardless of the concentration of copper present. The Δ*copA*::*erm-bar* and Δ*copA*::*bar* mutants showed the same degree of copper sensitivity (Fig. 3A).

To corroborate that the observed growth defects were due specifically to excess copper, we measured the growth of the Δ*copA*::*bar* mutant in the presence of copper, with and without the copper chelator bathocuproinedisulfonic acid (BCS). As expected, Δ*copA*::*bar* was unable to grow in the presence of 20 μM Cu^{2+}, whereas the WT is unaffected (Fig. 3B). However, growth of Δ*copA*::*bar* in the presence of copper was rescued by addition of 80 μM BCS (Fig. 3B), suggesting that free copper is indeed responsible for the observed lack of growth in the mutant. To verify that the absence of CopA was responsible for susceptibility to copper toxicity, we complemented *copA* at the chromosomal *att*Tn*7* site in the Δ*copA*::*bar* strain and observed that growth was rescued in the presence of copper (Fig. 3B). On the basis of these results, we conclude that CopA

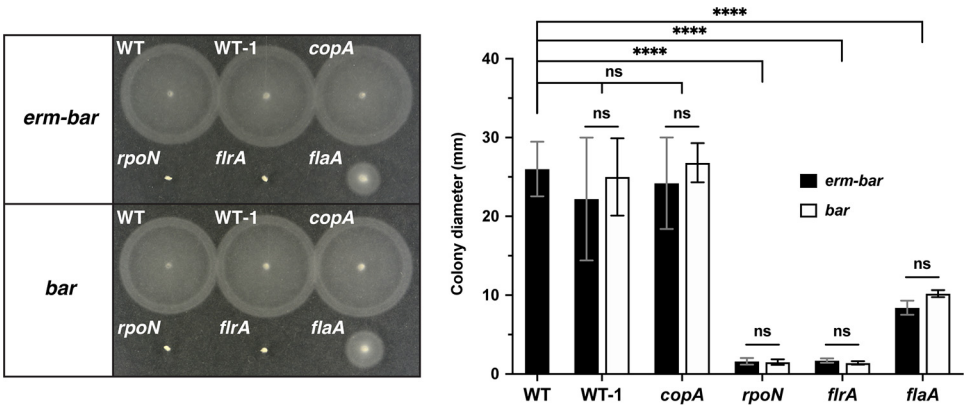

FIG 4 Assaying the phenotype of strains deleted for motility factors. Representative TBS agar trays showing the migration of strains from the inoculation point after incubation at 28°C for 4 h. WT is MJM1100 (ES114), while WT-1 represents the *att*Tn*7*-marked MJM1100 strain with barcode 1 (either WT::*erm-bar*1 or WT::*bar*1). Bar graph shows the quantified data from five independent replicates with error bars showing the standard deviations of the means ($n = 5$). Statistical analysis was performed using a two-way ANOVA test. ****, $P < 0.0001$.

is required for resistance to copper in *V. fischeri*, consistent with its function in other *Gammaproteobacteria* (48).

To further test our deletion method, we generated mutants in multiple genes required for *V. fischeri* motility—*rpoN*, *flrA*, and *flaA*—and tested the resulting strains' motility phenotypes on soft agar plates (28, 50, 51). We also included a WT strain tagged with the deletion scars at the *att*Tn*7* site (WT-1) and *copA* mutants as controls. While the motility of WT *V. fischeri* resulted in a migration disc with a diameter of 26 mm from the inoculation point on soft agar plates, deleting *flaA* resulted in a drastic reduction in migration (9 mm), while deleting either *flrA* or *rpoN* resulted in no motility (1.5 mm) (Fig. 4). We observed that both the *erm-bar* and *bar* versions of the gene deletions displayed equivalent phenotypes, showing that the strains behave as null alleles regardless of whether the scar contains the *erm* cassette (Fig. 4). The motility of both the WT-1 and *copA* strains is comparable to that of the WT, showing that motility defects are due to the deleted loci and not to the insertion of the deletion scars.

Removing the erythromycin resistance cassette minimizes polar effects of the barcoded deletions. While the presence or absence of the *erm* cassette does not prevent deletion strains from manifesting the corresponding phenotypes (Fig. 3A and 4), we were concerned about polar effects on downstream gene expression upon insertion of the 1,049-bp heterologous *erm* cassette (52–54). To test the effect of the *erm* cassette on downstream gene expression, we used reverse transcriptase quantitative PCR (RT-qPCR) to measure expression of genes immediately upstream and downstream of a targeted gene deletion for three different predicted operons. In each case, we measured the ratio in expression levels of the downstream versus upstream genes in the mutant, normalized to the ratio in WT *V. fischeri* (defining this normalized value as the "polarity ratio"). For both *rpoN* and *cheA*, deletion scars of either *erm-bar* or *bar* resulted in negligible changes in the polarity ratio (Fig. 5). In contrast, the polarity ratio of Δ*cusA*::*erm-bar* was 26-fold higher than WT, whereas removal of the *erm* cassette to form the in-frame deletion scar restored the polarity ratio to basal levels (Fig. 5). We conclude that, in at least some cases, *gene*::*bar* deletion scars can alleviate collateral effects on flanking genes that are caused by inserting an antibiotic resistance cassette.

Development of a computational pipeline to analyze *V. fischeri* BarSeq data. With the ability to quickly generate precise barcoded deletions, we next sought to compete the Δ*gene*::*bar* deletions en masse during host colonization. We therefore developed a BarSeq sample preparation protocol, and an accompanying computational package to analyze the data (Fig. 6). To accomplish this, we mixed barcoded strains to generate an input library (i.e., a synthetic microbiome). This library was then used to inoculate media and/or squid hatchlings, which were then sampled at the

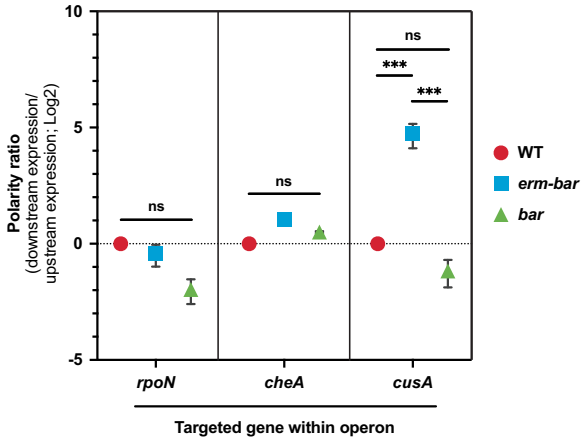

FIG 5 The *gene*::*bar* deletion scar reduces polar effects on gene expression introduced by the *erm* cassette. Graph showing the polarity ratio (expression of the downstream gene/expression of the upstream gene; relative to the indicated gene deletion target) for the indicated gene constructs within their respective predicted operons as measured by RT-qPCR. Statistical analysis was performed using a two-way ANOVA test. ***, $P < 0.001$.

desired time points. Samples were then processed to extract genomic DNA (gDNA), and PCR was performed with dual-index Illumina sequencing primers to obtain double-stranded DNA (dsDNA) fragments containing the barcoded deletion scars. The resulting library was then sequenced on an Illumina MiSeq and demultiplexed based on the unique dual indexes (55). The resulting sequence data were then analyzed using the barseq package, which identifies and counts the barcodes present in the samples, assigns strain identity, normalizes strain counts, and calculates relative frequency and the competitive index (CI) for each strain within the samples. The BarSeq protocol provides a streamlined and effective way to measure population dynamics throughout squid colonization.

BarSeq enables sensitive multiplex competition experiments. To test our BarSeq protocol in tracking individual strains within a population, we performed an *in vitro* competition and a competitive colonization experiment using an input library of seven different barcoded strains mixed in an equivalent ratio. In addition to several mutant strains, we included three WT::*bar* strains that had the *bar* scar inserted at the *att*Tn*7* site that could be similarly tracked using amplicon sequencing but without affecting the phenotypes of the strains (WT-1, WT-2, and WT-3 in Fig. 7). After 15 generations of growth *in vitro*, the proportion of most strains relative to the WT::*bar* strains remained stable except for *flrA* and *rpoN* deletion strains, which were fourfold higher and lower, respectively, compared to WT::*bar* (Fig. 7A). In contrast, following 48 h of squid colonization—which corresponds to approximately 15 bacterial generations (32)—we observed reduced levels of the *flaA* flagellin mutant and severely reduced levels of the *flrA*, *rpoN*, and *cheA* strains, all of which were near the limit of detection (Fig. 7B). This result is consistent with their previously known roles as necessary factors for squid colonization, although we did observe higher levels of *flaA* in the competitive colonization than are observed when a transposon insertion is competed against the wild-type strain (28, 50, 51, 56). We note that there was relatively little variability among the WT::*bar* strains in the analysis, whereas the 4- to 5-log-unit scale in which to identify colonization defects provided a substantially greater range over which to identify and refine colonization phenotypes *in vivo* (Fig. 7B). Taken together, these results show that our method for targeted barcoded deletions, multiplex squid colonization, and analysis by BarSeq allows for reproducible competition experiments *in vitro* and *in vivo* with high sensitivity.

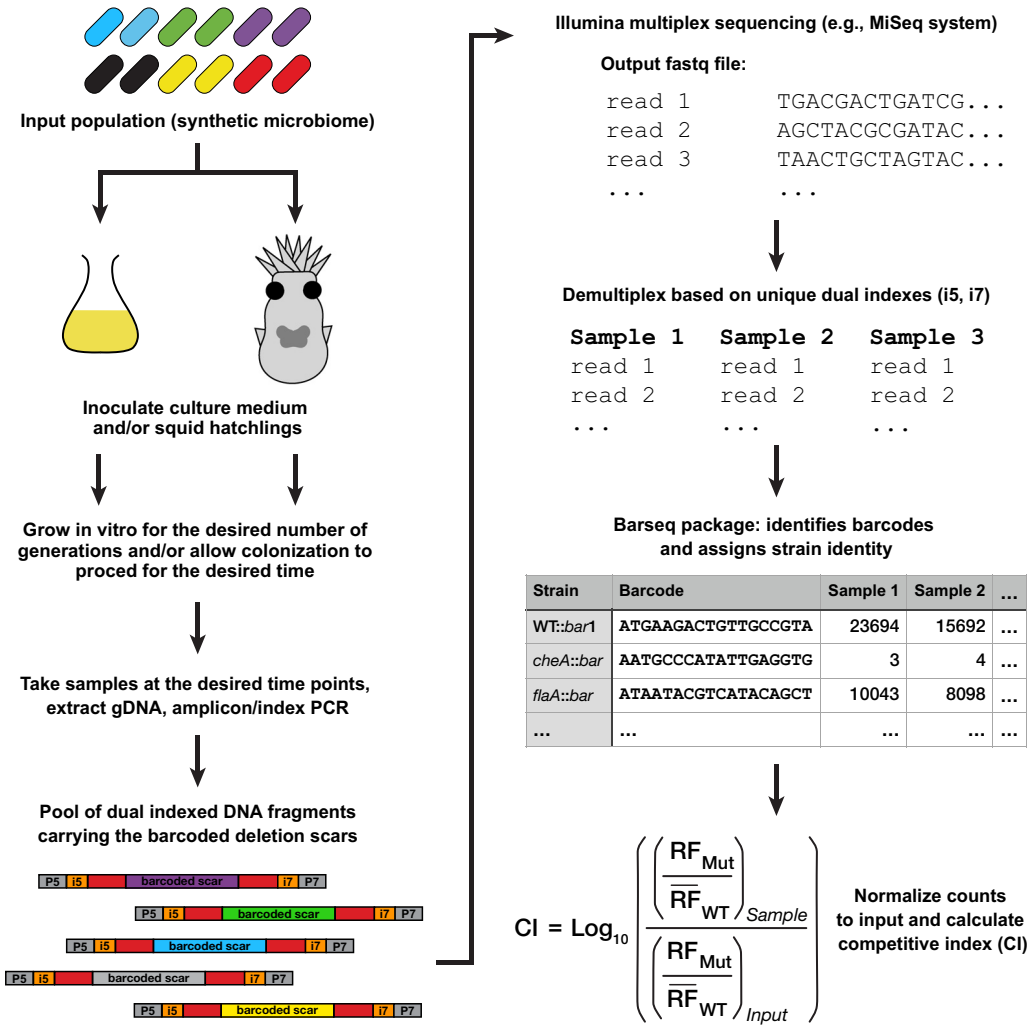

FIG 6 Overview of BarSeq experiments and computational package. Methodology and software for performing BarSeq experiments were described in the main text. An input population is used to inoculate squid or media, and samples are taken at the times of interest for gDNA extraction and processing to be sequenced by Illumina sequencing. The i5 and i7 segments are the index sequences in the dual indexed DNA fragments, whereas the P5 and P7 sequences are sequencing adapters for the MiSeq flow cell (details in Table S2). Sequencing reads are analyzed by the barseq package to obtain counts for individual strains in a sample based on their unique barcodes. Those counts are then used to calculate the relative frequencies of individual strains at each time point and the competitive index (CI) as described in Materials and Methods.

DISCUSSION

In this study, we developed a method to quickly generate gene deletions where the resulting strains are tagged with unique DNA barcodes. We demonstrated the utility of these strains in performing BarSeq high-throughput competitive colonization experiments and introduced a software package to analyze the resulting sequencing data. BarSeq provides a sensitive method to track population dynamics of squid colonization by *V. fischeri*.

Generation of targeted, barcoded gene deletions that minimize effects on neighboring genes. Our approach builds upon previous SOE-PCR/*tfoX* mutagenesis techniques to incorporate a unique barcode in each deletion strain, which enables high-throughput experiments via barcode sequencing (BarSeq). Since BarSeq relies on amplicon sequencing, library preparation is straightforward and allows for a large number of samples to be processed in parallel. The method we have employed to design the barcode and flanking sequences was planned to minimize disruption on flanking genes. Expression of bacterial genes is frequently organized by their genetic

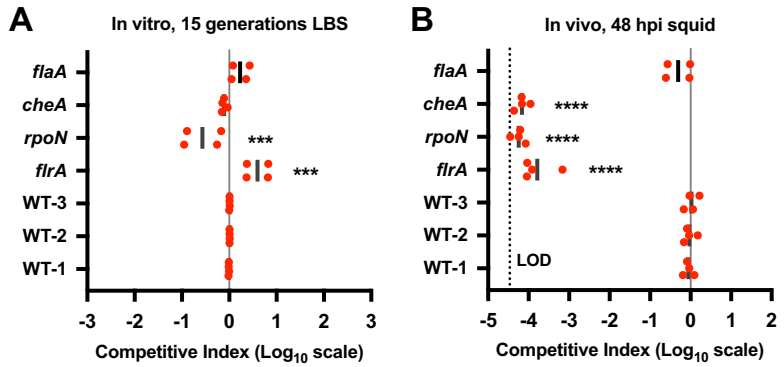

FIG 7 BarSeq enables high-throughput competition experiments. (A and B) Graphs show the mean competitive index (CI) on a $\log_{10}$ scale for each barcoded strain in the population using the WT strains as controls as described by Brooks et al. (79) after 15 generations *in vitro* in LBS (A) and 48 h post-squid inoculation (hours postinoculation [hpi]) (B). WT is MJM1100 (ES114). WT-1 represents the *att*Tn*7*-marked MJM1100 strain with barcode 1 (WT::*bar*1), and similarly for WT-2 and WT-3 for barcodes 2 and 3, respectively. LOD, limit of detection for the experiment (3.39×10^{-5}). Each symbol represents the value for one biological replicate. Statistical analysis was performed using a one-way ANOVA test comparing each strain to WT-1. ***, $P < 0.001$; ****, $P < 0.0001$.

arrangement into operons where expression of operon members is driven by a common promoter (57). However, given that some regulatory regions overlap in neighboring genes, deletion of one gene can alter the expression level of another nearby cistron. These off-target effects on gene expression could obfuscate the analysis of experimental results. Similar to the approach used by Baba et al. (53), our deletion approach reduces off-target effects on gene expression by ensuring the formation of an in-frame open reading frame within the deletion scar and including several codons at the end of the deletion target where the ribosome binding site of downstream genes is frequently located (Fig. 1B and Fig. 5). We do note a potential limitation any time that foreign codons are introduced. The rarest codon within the scar (normalized to the set of codons for that amino acid) comprises 2% of the arginines encoded in the genome. It is formally possible that under growth conditions not tested here, for example, a different tRNA pool in the cell could theoretically lead to distinct effects. Our polarity assay results suggest that this is not an issue under typical laboratory growth conditions (Fig. 5). Nonetheless, there may be conditions in which the introduced DNA leads to substantive effects.

BarSeq enables detailed studies of the molecular mechanisms that result in establishment of the *Vibrio*-squid symbiosis. Using an INSeq screen, our lab previously identified 344 putative novel squid colonization factors in *V. fischeri* (32). Our deletion approach, combined with BarSeq, will enable the high-throughput characterization of these factors during squid colonization by allowing multiplexing of colonization factor mutants and tracking of individual strains. By enabling a more precise study of colonization factors, BarSeq has several potential applications.

BarSeq can be applied to the study of strain variation and evolution of colonization mechanisms in the *Vibrio*-squid symbiosis. *V. fischeri* strain variation is an important consideration when studying the mechanisms of colonization of the squid LO (58, 59). Previous studies have shown that multiple strains can cocolonize the squid LO and that they do so at different rates (60–62). More recent studies have focused on deciphering the specific mechanisms that result in differing colonization behavior (63, 64). The barcode-tagged mutagenesis method presented here can be applied to generate uniquely tagged WT or mutant strains of the various phylogenetically distinct *V. fischeri* strains and assayed in multiplexed format during squid colonization using BarSeq. We have already successfully used our SOE-PCR/*tfoX* mutagenesis approach to make targeted deletions in strain SR5, showing that this method is applicable to *V. fischeri* strains that are evolutionarily distant to the frequently used ES114 strain (63).

BarSeq can also be used in directed evolution experiments to examine the functional evolution of colonization factors. Directed evolution experiments have recently been applied to study colonization factors in *V. fischeri* (65). The ease of tracking large numbers of individual *V. fischeri* strains using BarSeq could enable tracking of strain lineages in long-term evolution experiments, as has been conducted in other organisms (39, 42, 43).

Phenotypes of *rpoN* and *flrA* mutants during competitive growth in media. Both *rpoN* and *flrA* deletion strains showed a statistically significant fourfold decrease and increase, respectively, during competitive growth in media compared to WT (Fig. 7A). Due to the nature of the factors they encode, the observed growth defects are likely due to changes in energetic and nutritional requirements when *rpoN* and *flrA* are deleted. The *rpoN* gene encodes the alternative σ^{54} factor that is responsible for expression of various systems involved in squid colonization, including Syp biofilm formation, flagellar motility, and luminescence (51, 66, 67). Therefore, it is not surprising that deleting the gene encoding σ^{54} has pleiotropic effects on gene expression due to misregulation of the RpoN regulon and could reduce the ability of the mutant strain to effectively compete for growth *in vitro*, though further experiments are necessary to define the precise mechanism for the defect. FlrA is the σ^{54}-dependent transcription factor that activates expression of the flagellar biosynthesis cascade and is required for motility and squid colonization (50). The high energetic cost of expressing all genes related to flagellar biosynthesis (68), which in *V. cholerae* requires FlrA-dependent regulation of 52 genes (69) and in *V. fischeri* between 39 and 131 genes (28), is consistent with the observed increase in growth of the *flrA* deletion strain compared to WT during competitive growth in media (Fig. 7A). Nonetheless, even though the changes observed in competitive growth of the *rpoN* and *flrA* mutants *in vitro* are in opposing directions (less versus more growth, respectively), both are severely defective in squid colonization (Fig. 7B). Future experiments using BarSeq to probe bacterial growth *in vitro* and during colonization have the potential to elucidate heretofore hidden phenotypes.

Discrepancy in *flaA* colonization efficiency measured by BarSeq versus traditional competitive squid colonization experiments. In our BarSeq experiment, the known colonization factor *flaA* shows only a small (ca. twofold) colonization defect after 48 h post-squid inoculation (Fig. 7B). In contrast, Millikan and Ruby showed that a *flaA* deletion made by insertion of a Kan^r cassette is severely defective during competitive colonization against WT *V. fischeri* (56). Using confocal microscopy, their work showed that LO colonization by *flaA* is delayed compared to WT by ~8 h. However, because our competitive colonization experiment using BarSeq was done at 48 h postinoculation, this delayed colonization is not enough to explain the observed discrepancy. Previous work has shown that the concentration of *V fischeri* in the inoculum can affect the number of different strains that can cocolonize the squid LO (70). This raises the possibility that the inoculum amount or the ratio of strains within the synthetic microbiome might affect the observed colonization defect. To address this, future experiments should examine how inoculum amount and the ratio of mutant strains to WT within a synthetic barcode-tagged population affects colonization efficiency for the different strains in the population.

In summary, we provide a new method for constructing barcoded deletions of *V. fischeri* genes, we demonstrate the utility of this method for generating in-frame deletions and discovering new functions of squid colonization factors, and we combine this approach with a computational tool to conduct multiplex animal colonization assays using barcode sequencing.

MATERIALS AND METHODS

Bacterial strains, growth conditions, plasmids, and primers. Bacterial strains used in this study are listed in Table 1, with Table S1 in the supplemental material containing an extended Table 1 showing the oligonucleotides used to generate the specified barcode-tagged gene deletions. Plasmids are listed in Table 2, and DNA oligonucleotides are listed in Table S2. DNA oligonucleotides were synthesized by Integrated DNA Technologies (Coralville, IA), and Sanger DNA sequencing was performed through the

TABLE 1 Bacterial strains used in this study

Strain	Alias	Genotype or description	Reference(s) or source
V. fischeri strains			
MJM1100	ES114 (WT)	ES114	78, 80
MJM1538	ES114/pLostfoX	MJM1100/pLostfoX	32
MJM1902	*copA*::Tn*erm*	MJM1100 *copA*::Tn*erm*	32
MJM3400	Δ*copA*::pEVS79-Δ*copA*	MJM1100 Δ*copA*::pEVS79-Δ*copA*	This work
MJM3401	Δ*copA*	MJM1100 Δ*copA*	This work
MJM3529	Δ*copA*::*erm-bar*	MJM1100 Δ*copA*::*erm-bar*	This work
MJM3534	Δ*cusA*::*erm-bar*	MJM1100 Δ*cusA*::*erm-bar*	This work
MJM3543	Δ*copA*::*bar*	MJM1100 Δ*copA*::*bar*	This work
MJM3565	Δ*cusA*::*bar*	MJM1100 Δ*cusA*::*bar*	This work
MJM3620	WT::*erm-bar1*	MJM1100 IG(*yeiR-glmS*)::*erm-bar*1	This work
MJM3621	WT::*erm-bar2*	MJM1100 IG(*yeiR-glmS*)::*erm-bar*2	This work
MJM3622	WT::*erm-bar3*	MJM1100 IG(*yeiR-glmS*)::*erm-bar*3	This work
MJM3629	WT::*bar*1	MJM1100 IG(*yeiR-glmS*)::*bar*1	This work
MJM3630	WT::*bar2*	MJM1100 IG(*yeiR-glmS*)::*bar*2	This work
MJM3631	WT::*bar3*	MJM1100 IG(*yeiR-glmS*)::*bar*3	This work
MJM3785	Δ*flrA*::*erm-bar*	MJM1100 Δ*flrA*::*erm-bar*	This work
MJM3785	Δ*flaA*::*erm-bar*	MJM1100 Δ*flaA*::*erm-bar*	This work
MJM3786	Δ*rpoN*::*erm-bar*	MJM1100 Δ*rpoN*::*erm-bar*	This work
MJM3788	Δ*cheA*::*erm-bar*	MJM1100 Δ*cheA*::*erm-bar*	This work
MJM3790	Δ*copA*::*bar att*Tn*7*::*copA*	MJM1100 Δ*copA*::*bar att*Tn*7*::*copA*	This work
MJM3792	Δ*flrA*::*bar*	MJM1100 Δ*flrA*::*bar*	This work
MJM3795	Δ*flaA*::*bar*	MJM1100 Δ*flaA*::*bar*	This work
MJM3796	Δ*rpoN*::*bar*	MJM1100 Δ*rpoN*::*bar*	This work
MJM3798	Δ*cheA*::*bar*	MJM1100 Δ*cheA*::*bar*	This work
E. coli strains			
MJM534	CC118 λ*pir*/pEVS104	Δ(*ara-leu*) *araD* Δ*lacX74 galE galK phoA20 thi-1 rpsE rpoB argE*(Am) *recA1*, lysogenized with λ*pir*/pEVS104	33
MJM537	DH5α λ*pir*	F⁻ ϕ80*lacZ*ΔM15 Δ(*lacZYA-argF*)U169 *supE44 hsdR17* (r_K^- m_K^+) *endA1 recA1 gyrA96 thi-1 relA1 uidA*::*pir*$^+$	Laboratory stock
MJM570	DH5α/pEVS79	F⁻ ϕ80*lacZ*ΔM15 Δ(*lacZYA-argF*)U169 *supE44 hsdR17* (r_K^- m_K^+) *endA1 recA1 gyrA96 thi-1 relA1*/pEVS79	33
MJM637	S17-1 λ*pir*/pUX-BF13	*pro res hsdR17* (r_K^- m_K^+) *recA* with an integrated *RP4-2-Tc*::*Mu-Km*::Tn*7* λ*pir*/pUX-BF13	72, 73
MJM658	BW23474/pEVS107	Δ*lac-169 robA1 creC510 hsdR514 uidA*(ΔMluI)::*pir116 endA*(*BT33*) *recA1*/pEVS107	70
MJM3287	NEB5α/pHB1	F⁻ ϕ80*lacZ*ΔM15 Δ(*lacZYA-argF*)U169 *glnV44 hsdR17* (r_K^- m_K^+) *endA1 recA1 gyrA96 thi-1 relA1 fhuA2 phoA*/pHB1	63
MJM3288	DH5α λ*pir*/pHB2	MJM537/pHB2	This work
MJM3383	NEB5α/pHB3	F⁻ ϕ80*lacZ*ΔM15 Δ(*lacZYA-argF*)U169 *glnV44 hsdR17* (r_K^- m_K^+) *endA1 recA1 gyrA96 thi-1 relA1 fhuA2 phoA*/pHB3	This work
MJM3478	KV8052: π3813[a]/pKV496	*lacI*^{q} *thi-1 supE44 endA1 recA1 hsdR17 gyrA462 zei-298*::Tn*10* Δ*thyA*::(*erm-pir-116*)/pKV496	38, 71

[a]Thymidine auxotroph, growth conditions in Materials and Methods.

University of Wisconsin–Madison Biotechnology Center. *Escherichia coli* strains were grown in Luria-Bertani (LB) medium (per liter, 25 g Difco LB broth [BD], in distilled water) at 37°C with aeration. Unless otherwise indicated, *V. fischeri* strains were grown in Luria-Bertani salt (LBS) medium (per liter, 25 g Difco LB broth [BD], 10 g NaCl, and 50 ml 1 M Tris buffer [pH 7.0] in distilled water) at 25°C with aeration. When necessary, growth media was solidified by adding 15 g Bacto agar (BD) per liter. For growth of *V. fischeri*, antibiotics (Gold Biotechnology) were added at the following concentrations: 5 μg/ml erythromycin, 5 μg/ml or 2.5 μg/ml chloramphenicol as indicated, and 100 μg/ml kanamycin. For *E. coli*, the antibiotic concentrations used were 100 μg/ml carbenicillin, 25 μg/ml chloramphenicol, and 50 μg/ml kanamycin. The *E. coli* strain π3813 containing pKV496 is a thymidine auxotroph and was grown in LB with 50 μg/ml kanamycin supplemented with 0.3 mM thymidine (38, 71).

The unmarked deletion of *copA* in *V. fischeri* MJM1100 was made by allelic exchange as described previously (63). Briefly, 1.6-kb upstream (US) and 1.6-kb downstream (DS) sequences of *copA* were amplified by PCR using oligonucleotides HB44 and HB45 and oligonucleotides HB46 and HB47, respectively, and were cloned using Gibson Assembly (NEBuilder HiFi DNA assembly cloning kit) into the linearized vector pEVS79 (linearized using oligonucleotides HB52 and HB53) (Table S2). The Gibson mix was transformed into *E. coli* NEB5α chemically competent cells and selected on chloramphenicol. The resulting pEVS79-Δ*copA* candidates were screened using PCR with oligonucleotides HB54 and HB55 and

TABLE 2 Plasmids used in this study

Plasmid	Relevant properties	Reference or source
pEVS79	Vector backbone for deletion construct via allelic exchange; Cam^r	33
pEVS104	Conjugation helper plasmid; Kan^r	33
pEVS107	Mini-Tn*7* mobilizable vector; Erm^r (transposon); Kan^r	70
pKV496	pEVS79 containing the FLP recombinase; Kan^r	38
pLostfoX	*tfoX* overexpression vector; Cam^r	44
pUC19	Cloning vector; Carb^r	Laboratory stock
pUX-BF13	Tn*7* transposase helper plasmid (*tns* genes); Carb^r	72
pHB1	pUC19 containing the LL-FRT-*erm*-FRT-spacer sequence in the HindIII/BamHI site	63
pHB2	pEVS107 containing *copA* (including 191 bp upstream and 321 bp downstream of the *copA* ORF) at the AscI site	This work
pHB3	pEVS79 containing 1.6 kb upstream/1.6 kb downstream of *copA*	This work

confirmed by sequencing, generating pHB3, which was conjugated into *V. fischeri* MJM1100 (ES114) via triparental mating with MJM534, which contains the helper plasmid pEVS104 (33). Single recombinants of pHB3 into the chromosome were screened and selected by growth on chloramphenicol (MJM3400), and double recombinants were screened and selected by loss of the antibiotic resistance cassette and *copA* (MJM3401). The resulting constructs were verified by PCR and sequencing (Table S2).

The *copA* gene was inserted into the *att*Tn*7* site in the chromosome using pEVS107 (70). The *copA* gene including 191-bp US and 321-bp DS sequences was amplified by PCR using oligonucleotides HB27 and HB34, and the product was digested with AscI and cloned into the AscI site of pEVS107. The resulting plasmid, pHB2 (pEVS107-*copA*), was transformed into and maintained in *E. coli* DH5α λ*pir* cells and verified by PCR (Table S2) and sequencing. pHB2 was conjugated into Δ*copA* strain (MJM3401) via tetraparental mating with donor MJM3288 (DH5α λ*pir*/pHB2), helper strains MJM637 (S17-1 λ*pir*/pUX-BF13) (72, 73) and MJM534 (CC118 λ*pir*/pEVS104) (33), and the recipient MJM3543 (Δ*copA*::*bar*), resulting in MJM3790 (Δ*copA*::*bar att*Tn*7*::*copA*). Candidates were confirmed by PCR (Table S2) and sequencing.

Construction of barcode-tagged gene deletions. The deletion protocol demonstrated in Fig. 1A is based on splicing by overlap extension PCR (SOE-PCR) and *tfoX* transformation (38, 44–46) to directly delete and tag targeted genes with a randomized sequence (barcode). Our protocol was in development prior to publication of the previous method (38), so while it is conceptually similar, the sequences of the linkers and primers are distinct. First, several oligonucleotides were designed specific to the targeted genes to amplify 1 kb of US (F1 and R1-LL) and DS (F2-RL and R2) DNA tagged with the left linker (LL) and right linker (RL) sequences, respectively, to screen the deletion scar via PCR (FO and RO), and to assay for the absence of the targeted gene (FW and RW) (Fig. 1A, Table S1, and Table S2). FW and RW were designed to amplify a fragment of 500 to 1,000 bp, depending on the size of the gene. The F1 and R2 oligonucleotides were designed to anneal 1-kb US and DS, respectively, of the targeted gene. The R1 oligonucleotide was designed to anneal starting at the start codon of the targeted open reading frame (ORF) going upstream, then the reverse complement of the LL sequence (LL reverse complement, 5′-CTGGCGAAGCATATATAAGAAGCTCGTCTCGT-3′) was attached to the 5′ end of the R1 oligonucleotide, resulting in R1-LL. The F2 oligonucleotide was designed to anneal at the last seven codons (6 amino acids [aa] and stop codon) on the 3′ end of the targeted ORF going downstream, then the RL sequence (RL, 5′-GACTTGACCTGGATGTCTCTACCCACAAGATCG-3′) was attached to the 5′ end of the F2 oligonucleotide, resulting in F2-RL. The FO and RO oligonucleotides (forward outside and reverse outside, respectively) were designed to anneal 500 bp away from the annealing sites of F1 and R2, respectively, and were used to probe the targeted genomic region for insertion of the desired deletion scar.

The middle dsDNA fragment containing the *erm* cassette flanked by FRT sites and the randomized barcode was obtained by PCR with Phusion Hot Start Flex 2× master mix (New England BioLabs [NEB]; catalog no. M0536L) and pHB1 as the template, which contains the LL-FRT-*erm*-FRT-spacer sequences and was built as described previously (63), and oligonucleotides HB42 and HB154. Oligonucleotide HB154 is a reverse primer and contains the RL sequence, 18 bp of randomized sequence composed of six trimers of "NNB" to prevent formation of stop codons (results in "VNN" codons in the forward direction), and the spacer sequence (Table S2). The resulting 1,049-bp product containing LL-FRT-*erm*-FRT-spacer-random barcode-RL was purified by gel extraction using a QIAquick gel extraction kit (Qiagen; catalog no. 28706). The flanking 1-kb US and DS fragments for each targeted gene were then fused to this middle DNA fragment via the homology between the LL and RL sequences and using SOE-PCR with the F1 and R2 oligonucleotides, resulting in the 3-kb mutagenic dsDNA. The reaction mixture contained 10 ng of each of the middle, US, and DS DNA fragments, 200 nM concentration of the corresponding F1 and R2 oligonucleotides (Table S2), 1× Phusion Hot Start Flex Master Mix (NEB; catalog no. M0536L), and H_2O up to a total volume of 25 μl. SOE-PCR conditions were 98°C for 30 s, 30 cycles with each cycle consisting of 98°C for 5 s, 60°C for 20 s, and 72°C for 1 min, with a final extension step at 72°C for 5 min.

The 3-kb mutagenic DNA fragments were purified using a QIAquick PCR purification kit (Qiagen; catalog no. 28106) and transformed into *V. fischeri* ES114 via natural transformation with pLostfoX (MJM1538) (32, 44) where the flanking sequences guide the barcoded *erm* cassette to substitute the targeted gene. Mutant candidates were selected on LBS with 5 μg/ml erythromycin (LBS-Erm5) and screened by PCR with oligonucleotide pairs F1/R2, FO/HB8, and FW/RW (as shown in Fig. 2A). The insertion of the *erm-bar* scar was confirmed by Sanger sequencing with primers HB8, HB9, HB42, and HB146, and the unique barcode sequence was recorded for each strain.

The final *bar* scars were made by triparental mating of donor MJM3478 (π3813/pKV496) (38) and helper strain MJM534 (CC118 λ*pir*/pEVS104) into recipient *V. fischeri* strains containing the *erm-bar* scar and selection on LBS containing 100 μg/ml kanamycin (LBS-Kan100). Plasmid pKV496 contains the FLP recombinase that removes the *erm* cassette and fuses the two surrounding FRT sites into one, resulting in the final *bar* scar as shown in Fig. 1B. The plasmid was eliminated by growing the candidates on LBS without selection twice and selecting colonies that were Erm^s and Kan^s. The *gene*::*bar* candidates were screened by PCR using oligonucleotide pairs F1/R2, FO/HB146 (RL), and FW/RW, and the deletion scar was verified by Sanger sequencing using oligonucleotides HB42 and HB146. The barcode sequences were verified to match the barcode within the parental strains containing the *gene*::*erm-bar* scar.

The barcoded WT *V. fischeri* strains (WT::*bar*) were constructed using the same procedure as outlined above for the gene deletions but targeting a site next to the *att*Tn*7* site in the intergenic region of *yeiR* and *glmS*. The 1-kb US and DS arms were amplified using PCR with ES114 gDNA and oligonucleotide pairs HB239/HB240 and HB241/HB242. After SOE-PCR to form the mutagenic DNA and *tfoX* transformation, the WT::*erm-bar* candidates were screened by PCR with oligonucleotide pairs HB243/HB244 and HB243/HB8. Sanger sequencing was used to confirm insertion of the *erm-bar* scar and record the unique barcode sequences. Triparental mating as described above was performed to remove the *erm* cassette using pKV496. The *bar* scar was confirmed by PCR with HB243/HB146 and Sanger sequencing.

Growth assays in the presence of copper. Colonies from freshly streaked LBS plates of the indicated *V. fischeri* strains were inoculated into 3 ml LBS with the appropriate antibiotics and grown for 8 h at 25°C with shaking. Three microliters of the LBS cultures was subcultured into 3 ml Tris minimal medium [per liter, 500 ml defined seawater (DSW; 2X), 50 ml of 1 M Tris base [pH 7.5], 1 ml of 5.8% K_2HPO_4, 1 ml of 10 mM $FeSO_4$, and 20 ml of 10% *N*-acetylglucosamine (GlcNAc), in distilled water; DSW (2×) = 100 mM $MgSO_4$, 20 mM $CaCl_2$, 600 mM NaCl, and 20 mM KCl] and incubated at 25°C overnight for ≤16 h. Overnight cultures were diluted to an optical density at 600 nm (OD_{600}) of 0.5 in 200 μl, and then 2 μl of solution with an OD_{600} of 0.5 was transferred into 198 μl of fresh Tris minimal medium containing the appropriate amounts of copper and/or bathocuproinedisulfonic acid (BCS) in a 96-well plate. The plate was then incubated in a Synergy Neo2 Multi-Mode microplate reader (BioTek) at 25°C with OD_{600} measurements every 15 min for 20 h. Copper stock solutions (100 mM) were prepared from copper(II) sulfate pentahydrate ($CuSO_4{\cdot}5H_2O$; Sigma-Aldrich; catalog no. 203165) and BCS stock solutions (50 mM) from bathocuproinedisulfonic acid disodium salt (Sigma-Aldrich; catalog no. B1125).

Motility assays. The indicated bacterial strains were streaked onto fresh LBS plates with the appropriate antibiotics and grown overnight at 25°C. Single colonies were picked with a sterile toothpick and deposited onto OmniTrays (Thermo Fisher Scientific; catalog no. 242811) containing TBS agar (per liter, 10 g Gibco Bacto tryptone [Thermo Fisher Scientific; catalog no. 211705], 50 ml of 1 M Tris buffer [pH 7.] 0, 20 g NaCl, 8.63 g MgSO4, and 3 g agar, in distilled water) by stabbing the toothpick into the media at a single spot. The trays were incubated at 28°C for 4 h, and the outer diameter of swimming cells was measured.

Measuring polarity ratio via RT-qPCR. The indicated bacterial strains were grown in 3 ml LBS with the appropriate antibiotics and grown at 25°C overnight. On the day of the experiment, 15 μl of the overnight cultures was transferred into 3 ml of fresh LBS, and growth was continued at 25°C with aeration. Samples were harvested at an OD_{600} of 0.2 to 0.4 (mid-log phase) by transferring 800 μl of culture into a 2-ml screw-cap tube containing 100 μl of a cold 95% ethanol (EtOH)–5% phenol solution that inactivates RNases (74). RNA extraction and RT-qPCR were performed as described previously (75). Briefly, cells were lysed in Tris-EDTA (TE) buffer (10 mM Tris-Cl [pH 8.0], 1 mM EDTA) containing lysozyme (Epicentre; catalog no. R1804M) and 1% sodium dodecyl sulfate (SDS). RNA was extracted using the hot phenol method (74) and digested with DNase I (NEB; catalog no. M0303S).

cDNA was synthesized from 0.5 μg of total RNA using the iScript Advanced cDNA synthesis kit (Bio-Rad; catalog no. 1725037) following the protocol 25°C for 5 min, 46°C for 20 min, and 95°C for 1 min. Quantitative PCR was performed using 1:10 dilutions of cDNA synthesis products with the iTaq Universal SYBR green supermix (Bio-Rad; catalog no. 1725121) on a CFX Connect real-time PCR detection system (Bio-Rad). The qPCR protocol was 95°C for 30 s and 40 cycles, with each cycle consisting of 95°C for 5 s and 58°C for 30 s with a final melt curve analysis to ensure specificity in the reaction. The mRNA levels of *rpoD*, *lptB*, *hpf*, *cheZ*, *cheB*, *cusB*, and *cusF* were measured using the oligonucleotide pairs listed in Table S2. Expression levels for each gene were normalized to that of *rpoD*, and the mutants were normalized to WT using the $2^{-\Delta\Delta CT}$ method (76). The polarity ratio of *rpoN*, *cheA*, and *cusA* was calculated as "expression of the downstream gene/expression of the upstream gene" using the respective flanking genes in each putative operon–*lptB-rpoN-hpf*, *cheZ-cheA-cheB*, and *cusB-cusA-cusF*. Operons were predicted using the BioCyc database for "*Aliivibrio fischeri* strain ES114, version 24.1," which is based on the sequenced genome in Mandel et al. (77, 78).

barseq bioinformatic tool. To quantify barcodes within each sequenced sample, we developed barseq (https://github.com/mjmlab/barseq), a python package that identifies putative barcodes in the sequenced reads and matches them to a user-provided barcode library. The program iterates through each sample and uses regular expressions to search within the reads for flanking sequences on the left (GCTCATGCACTTGATTCC; spacer sequence) and the right (GACTTGACCTGGATGTCT; right linker sequence) of the barcode (Fig. 1B), while also allowing for 18 random nucleotides that represent a candidate barcode. The putative barcode sequence is then mapped against the reference barcode library and increases the count for the matched strain. barseq outputs a tab-delimited table with the barcode/strain counts for each of the samples analyzed.

Barcode sequencing and multiplexed competitive experiments. Cells of the indicated strains (Fig. 7) were grown in 3 ml LBS at 25°C overnight with aeration. The cultures were then diluted (1:80)

into 3 ml fresh LBS and grown to mid-log phase (OD_{600} of 0.2). Equivalent ODs of cells from each strain [volume to mix calculated as volume (in microliters) = $(1.25/OD_{600}) \times 50$] were mixed, resulting in a multiplexed population with each strain present at a 1-to-1 ratio. A sample from this input library was harvested by collecting cells from 700 μl by centrifugation and storing the cell pellet at −80°C. The input library was then used to inoculate hatchling *Euprymna scolopes* squid at 5×10^3 to 9×10^3 CFU/ml for 3 h in FSIO (filter-sterilized Instant Ocean) as previously described (20). Squid samples ($n = 24$, per replicate) were harvested at 48 h postinoculation and surface sterilized by storing at −80°C. Concurrently to squid colonization, the input library was competed for growth *in vitro* for 15 generations by diluting the library 1:181 into LBS, growing at 25°C with aeration back to the starting OD_{600}, repeating this process once more, and harvesting samples as described above. Individual squid were homogenized in 700 μl of FSIO, 500 μl of each homogenate was mixed in a 50-ml conical tube, diluted 1:20 in 70% IO (Instant Ocean), and 50 μl plated onto LBS plates in triplicate. After a 17-h overnight incubation at 25°C, the bacterial colonies from each plate were scraped with a sterile cell scraper into 1 ml of 70% IO and collected by centrifugation. Cell pellets were stored at −20°C prior to DNA extraction.

Genomic DNA from the cell pellets was extracted and purified using the Qiagen DNeasy blood and tissue kit (Qiagen; catalog no. 69506) following the Gram-negative bacteria protocol and quantified using a NanoDrop spectrophotometer (Thermo Fisher Scientific). The barcoded scars were amplified together with dual-index Illumina sequencing primers (55). The reaction mixtures contained 50 ng of gDNA, 200 nM each oligonucleotide (Table S2), 1× Phusion Hot Start Flex Master Mix (NEB; catalog no. M0536L), and H_2O up to a total volume of 50 μl. PCR conditions were 98°C for 30 s, 20 cycles with each cycle consisting of 98°C for 10 s, 60°C for 10 s, and 72°C for 10 s, with a final extension step at 72°C for 5 min. PCR products were visualized using a 2% agarose gel to confirm the dual-indexed amplicon of 231 bp and purified using a QIAquick PCR purification kit (Qiagen; catalog no. 28106). Purified PCR products were quantified using a Qubit 3 fluorometer (Life Technologies), pooled in equimolar amounts, and diluted to 4 nM. The pool was sequenced on an Illumina MiSeq using the 2×250 bp v2 kit with a 10% PhiX control following the manufacturer's protocol (Illumina, Inc., San Diego, CA) and using custom primers developed from reference 55. The sequencing data were processed using the barseq python package to obtain strain counts per sample, and mutants that were in the input library but still being validated were removed from the data set. The relative frequency (RF) for each strain in a sample was calculated, normalized to the RF in the input library and the average RF in the sample, and the competitive index (CI) was then calculated using the formula: $CI = \log_{10} [(RF_{mutant}/\text{average } RF_{WT})_{Sample}/(RF_{mutant}/\text{average } RF_{WT})_{Input}]$.

SUPPLEMENTAL MATERIAL

Supplemental material is available online only.

TABLE S1, XLSX file, 0.01 MB.

TABLE S2, XLSX file, 0.02 MB.

TABLE S3, XLSX file, 0.01 MB.

ACKNOWLEDGMENTS

We thank Karen L. Visick for plasmid pKV496 and members of the Mandel lab for comments on the mutagenesis protocol and manuscript.

This work was funded by NIGMS grant R35 GM119627 to M.J.M., an American Society for Microbiology Undergraduate Research Fellowship to E.F.B., and the McNair Scholars Program (E.F.B.). G.S. acknowledges support from the USDA National Institute of Food and Agriculture (NIFA), Agricultural and Food Research Initiative (AFRI) Foundation grant 2020-67015-31576, and USDA NIFA HATCH grant WIS02007.

REFERENCES

1. Taschuk R, Griebel PJ. 2012. Commensal microbiome effects on mucosal immune system development in the ruminant gastrointestinal tract. Anim Health Res Rev 13:129–141. https://doi.org/10.1017/S1466252312000096.
2. Montgomery MK, McFall-Ngai M. 1994. Bacterial symbionts induce host organ morphogenesis during early postembryonic development of the squid *Euprymna scolopes*. Development 120:1719–1729.
3. Shropshire JD, Bordenstein SR. 2016. Speciation by symbiosis: the microbiome and behavior. mBio 7:e01785-15. https://doi.org/10.1128/mBio.01785-15.
4. Honda K, Littman DR. 2012. The microbiome in infectious disease and inflammation. Annu Rev Immunol 30:759–795. https://doi.org/10.1146/annurev-immunol-020711-074937.
5. Byrd AL, Belkaid Y, Segre JA. 2018. The human skin microbiome. Nat Rev Microbiol 16:143–155. https://doi.org/10.1038/nrmicro.2017.157.
6. O'Dwyer DN, Dickson RP, Moore BB. 2016. The lung microbiome, immunity, and the pathogenesis of chronic lung disease. J Immunol 196:4839–4847. https://doi.org/10.4049/jimmunol.1600279.
7. Aragón IM, Herrera-Imbroda B, Queipo-Ortuño MI, Castillo E, Del Moral JS-G, Gómez-Millán J, Yucel G, Lara MF. 2018. The urinary tract microbiome in health and disease. Eur Urol Focus 4:128–138. https://doi.org/10.1016/j.euf.2016.11.001.
8. Kinross JM, Darzi AW, Nicholson JK. 2011. Gut microbiome-host interactions in health and disease. Genome Med 3:14. https://doi.org/10.1186/gm228.
9. Parfrey LW, Knight R. 2012. Spatial and temporal variability of the human microbiota. Clin Microbiol Infect 18(Suppl 4):8–11. https://doi.org/10.1111/j.1469-0691.2012.03861.x.
10. Costello EK, Lauber CL, Hamady M, Fierer N, Gordon JI, Knight R. 2009. Bacterial community variation in human body habitats across space and time. Science 326:1694–1697. https://doi.org/10.1126/science.1177486.
11. Kostic AD, Howitt MR, Garrett WS. 2013. Exploring host-microbiota

interactions in animal models and humans. Genes Dev 27:701–718. https://doi.org/10.1101/gad.212522.112.
12. Ruby EG. 1999. The *Euprymna scolopes-Vibrio fischeri* symbiosis: a biomedical model for the study of bacterial colonization of animal tissue. J Mol Microbiol Biotechnol 1:13–21.
13. McFall-Ngai M. 2008. The squid-vibrio association – a naturally occurring, experimental model of animal/bacterial partnerships, p 102–112. In Huffnagle GB, Noverr MC (ed), GI microbiota and regulation of the immune system. Springer Science+Business Media, New York, NY.
14. McFall-Ngai MJ. 2014. The importance of microbes in animal development: lessons from the squid-vibrio symbiosis. Annu Rev Microbiol 68:177–194. https://doi.org/10.1146/annurev-micro-091313-103654.
15. Tischler AH, Hodge-Hanson KM, Visick KL. 2019. *Vibrio fischeri*–squid symbiosis. Elsevier Oceanogr Ser 267:1–9.
16. McFall-Ngai M. 2014. Divining the essence of symbiosis: insights from the squid-vibrio model. PLoS Biol 12:e1001783. https://doi.org/10.1371/journal.pbio.1001783.
17. Nyholm SV, McFall-Ngai M. 2004. The winnowing: establishing the squid–vibrio symbiosis. Nat Rev Microbiol 2:632–642. https://doi.org/10.1038/nrmicro957.
18. Jones BW, Nishiguchi MK. 2004. Counterillumination in the Hawaiian bobtail squid, *Euprymna scolopes* Berry (Mollusca: Cephalopoda). Mar Biol 144:1151–1155. https://doi.org/10.1007/s00227-003-1285-3.
19. Lee KH, Ruby EG. 1994. Effect of the squid host on the abundance and distribution of symbiotic *Vibrio fischeri* in nature. Appl Environ Microbiol 60:1565–1571. https://doi.org/10.1128/AEM.60.5.1565-1571.1994.
20. Naughton LM, Mandel MJ. 2012. Colonization of *Euprymna scolopes* squid by *Vibrio fischeri*. J Vis Exp 2012:e3758. https://doi.org/10.3791/3758.
21. Mandel MJ, Schaefer AL, Brennan CA, Heath-Heckman EAC, DeLoney-Marino CR, McFall-Ngai MJ, Ruby EG. 2012. Squid-derived chitin oligosaccharides are a chemotactic signal during colonization by *Vibrio fischeri*. Appl Environ Microbiol 78:4620–4626. https://doi.org/10.1128/AEM.00377-12.
22. Essock-Burns T, Bongrand C, Goldman WE, Ruby EG, McFall-Ngai MJ. 2020. Interactions of symbiotic partners drive the development of a complex biogeography in the squid-vibrio symbiosis. mBio 11:e00853-20. https://doi.org/10.1128/mBio.00853-20.
23. Sycuro LK, Ruby EG, McFall-Ngai M. 2006. Confocal microscopy of the light organ crypts in juvenile *Euprymna scolopes* reveals their morphological complexity and dynamic function in symbiosis. J Morphol 267:555–568. https://doi.org/10.1002/jmor.10422.
24. Nyholm SV, Deplancke B, Gaskins HR, Apicella MA, McFall-Ngai MJ. 2002. Roles of *Vibrio fischeri* and nonsymbiotic bacteria in the dynamics of mucus secretion during symbiont colonization of the *Euprymna scolopes* light organ. Appl Environ Microbiol 68:5113–5122. https://doi.org/10.1128/aem.68.10.5113-5122.2002.
25. Nyholm SV, Stabb EV, Ruby EG, McFall-Ngai MJ. 2000. Establishment of an animal–bacterial association: recruiting symbiotic vibrios from the environment. Proc Natl Acad Sci U S A 97:10231–10235. https://doi.org/10.1073/pnas.97.18.10231.
26. Altura MA, Heath-Heckman EAC, Gillette A, Kremer N, Krachler A-M, Brennan C, Ruby EG, Orth K, McFall-Ngai MJ. 2013. The first engagement of partners in the *Euprymna scolopes-Vibrio fischeri* symbiosis is a two-step process initiated by a few environmental symbiont cells. Environ Microbiol 15:2937–2950. https://doi.org/10.1111/1462-2920.12179.
27. Visick KL. 2009. An intricate network of regulators controls biofilm formation and colonization by *Vibrio fischeri*. Mol Microbiol 74:782–789. https://doi.org/10.1111/j.1365-2958.2009.06899.x.
28. Brennan CA, Mandel MJ, Gyllborg MC, Thomasgard KA, Ruby EG. 2013. Genetic determinants of swimming motility in the squid light-organ symbiont *Vibrio fischeri*. Microbiologyopen 2:576–594. https://doi.org/10.1002/mbo3.96.
29. Stabb EV, Schaefer A, Bose JL, Ruby EG. 2008. Quorum signaling and symbiosis in the marine luminous bacterium *Vibrio fischeri*, p 233–250. In Winans SC, Bassler BL (ed), Chemical communication among bacteria. American Society for Microbiology, Washington, DC.
30. Visick KL, Foster J, Doino J, McFall-Ngai M, Ruby EG. 2000. *Vibrio fischeri lux* genes play an important role in colonization and development of the host light organ. J Bacteriol 182:4578–4586. https://doi.org/10.1128/jb.182.16.4578-4586.2000.
31. Lupp C, Urbanowski M, Greenberg EP, Ruby EG. 2003. The *Vibrio fischeri* quorum-sensing systems *ain* and *lux* sequentially induce luminescence gene expression and are important for persistence in the squid host. Mol Microbiol 50:319–331. https://doi.org/10.1046/j.1365-2958.2003.t01-1-03585.x.
32. Brooks JF, II, Gyllborg MC, Cronin DC, Quillin SJ, Mallama CA, Foxall R, Whistler C, Goodman AL, Mandel MJ. 2014. Global discovery of colonization determinants in the squid symbiont *Vibrio fischeri*. Proc Natl Acad Sci U S A 111:17284–17289. https://doi.org/10.1073/pnas.1415957111.
33. Stabb EV, Ruby EG. 2002. RP4-based plasmids for conjugation between *Escherichia coli* and members of the Vibrionaceae. Methods Enzymol 358:413–426. https://doi.org/10.1016/s0076-6879(02)58106-4.
34. Lyell NL, Dunn AK, Bose JL, Stabb EV. 2010. Bright mutants of *Vibrio fischeri* ES114 reveal conditions and regulators that control bioluminescence and expression of the *lux* operon. J Bacteriol 192:5103–5114. https://doi.org/10.1128/JB.00524-10.
35. Baym M, Shaket L, Anzai IA, Adesina O, Barstow B. 2016. Rapid construction of a whole-genome transposon insertion collection for *Shewanella oneidensis* by Knockout Sudoku. Nat Commun 7:13270. https://doi.org/10.1038/ncomms13270.
36. Goodman AL, McNulty NP, Zhao Y, Leip D, Mitra RD, Lozupone CA, Knight R, Gordon JI. 2009. Identifying genetic determinants needed to establish a human gut symbiont in its habitat. Cell Host Microbe 6:279–289. https://doi.org/10.1016/j.chom.2009.08.003.
37. Studer SV, Mandel MJ, Ruby EG. 2008. AinS quorum sensing regulates the *Vibrio fischeri* acetate switch. J Bacteriol 190:5915–5923. https://doi.org/10.1128/JB.00148-08.
38. Visick KL, Hodge-Hanson KM, Tischler AH, Bennett AK, Mastrodomenico V. 2018. Tools for rapid genetic engineering of *Vibrio fischeri*. Appl Environ Microbiol 84:e00850-18. https://doi.org/10.1128/AEM.00850-18.
39. Jahn LJ, Porse A, Munck C, Simon D, Volkova S, Sommer MOA. 2018. Chromosomal barcoding as a tool for multiplexed phenotypic characterization of laboratory evolved lineages. Sci Rep 8:6961. https://doi.org/10.1038/s41598-018-25201-5.
40. Smith AM, Heisler LE, Mellor J, Kaper F, Thompson MJ, Chee M, Roth FP, Giaever G, Nislow C. 2009. Quantitative phenotyping via deep barcode sequencing. Genome Res 19:1836–1842. https://doi.org/10.1101/gr.093955.109.
41. Robinson DG, Chen W, Storey JD, Gresham D. 2014. Design and analysis of Bar-seq experiments. G3 (Bethesda) 4:11–18. https://doi.org/10.1534/g3.113.008565.
42. Blundell JR, Levy SF. 2014. Beyond genome sequencing: lineage tracking with barcodes to study the dynamics of evolution, infection, and cancer. Genomics 104:417–430. https://doi.org/10.1016/j.ygeno.2014.09.005.
43. Abel S, Abel Zur Wiesch P, Chang H-H, Davis BM, Lipsitch M, Waldor MK. 2015. Sequence tag-based analysis of microbial population dynamics. Nat Methods 12:223–226. https://doi.org/10.1038/nmeth.3253.
44. Pollack-Berti A, Wollenberg MS, Ruby EG. 2010. Natural transformation of *Vibrio fischeri* requires *tfoX* and *tfoY*. Environ Microbiol 12:2302–2311. https://doi.org/10.1111/j.1462-2920.2010.02250.x.
45. De Souza Silva O, Blokesch M. 2010. Genetic manipulation of *Vibrio cholerae* by combining natural transformation with FLP recombination. Plasmid 64:186–195. https://doi.org/10.1016/j.plasmid.2010.08.001.
46. Dalia AB, Lazinski DW, Camilli A. 2013. Characterization of undermethylated sites in *Vibrio cholerae*. J Bacteriol 195:2389–2399. https://doi.org/10.1128/JB.02112-12.
47. Baba T, Mori H. 2008. The construction of systematic in-frame, single-gene knockout mutant collection in *Escherichia coli* K-12, p 171–181. In Osterman AL, Gerdes SY (ed), Microbial gene essentiality: protocols and bioinformatics. Humana Press, Totowa, NJ.
48. Hernández-Montes G, Argüello JM, Valderrama B. 2012. Evolution and diversity of periplasmic proteins involved in copper homeostasis in gamma proteobacteria. BMC Microbiol 12:249. https://doi.org/10.1186/1471-2180-12-249.
49. Rensing C, Fan B, Sharma R, Mitra B, Rosen BP. 2000. CopA: an *Escherichia coli* Cu(I)-translocating P-type ATPase. Proc Natl Acad Sci U S A 97:652–656. https://doi.org/10.1073/pnas.97.2.652.
50. Millikan DS, Ruby EG. 2003. FlrA, a σ^{54}-dependent transcriptional activator in *Vibrio fischeri*, is required for motility and symbiotic light-organ colonization. J Bacteriol 185:3547–3557. https://doi.org/10.1128/jb.185.12.3547-3557.2003.
51. Wolfe AJ, Millikan DS, Campbell JM, Visick KL. 2004. *Vibrio fischeri* σ^{54} controls motility, biofilm formation, luminescence, and colonization. Appl Environ Microbiol 70:2520–2524. https://doi.org/10.1128/aem.70.4.2520-2524.2004.
52. Raynal A, Karray F, Tuphile K, Darbon-Rongère E, Pernodet J-L. 2006. Excisable cassettes: new tools for functional analysis of *Streptomyces* genomes. Appl Environ Microbiol 72:4839–4844. https://doi.org/10.1128/AEM.00167-06.
53. Baba T, Ara T, Hasegawa M, Takai Y, Okumura Y, Baba M, Datsenko KA, Tomita M, Wanner BL, Mori H. 2006. Construction of *Escherichia coli* K-12

in-frame, single-gene knockout mutants: the Keio collection. Mol Syst Biol 2:2006.0008. https://doi.org/10.1038/msb4100050.
54. Oppenheim DS, Yanofsky C. 1980. Translational coupling during expression of the tryptophan operon of *Escherichia coli*. Genetics 95:785–795.
55. Kozich JJ, Westcott SL, Baxter NT, Highlander SK, Schloss PD. 2013. Development of a dual-index sequencing strategy and curation pipeline for analyzing amplicon sequence data on the MiSeq Illumina sequencing platform. Appl Environ Microbiol 79:5112–5120. https://doi.org/10.1128/AEM.01043-13.
56. Millikan DS, Ruby EG. 2004. *Vibrio fischeri* flagellin A is essential for normal motility and for symbiotic competence during initial squid light organ colonization. J Bacteriol 186:4315–4325. https://doi.org/10.1128/JB.186.13.4315-4325.2004.
57. Koonin EV. 2009. Evolution of genome architecture. Int J Biochem Cell Biol 41:298–306. https://doi.org/10.1016/j.biocel.2008.09.015.
58. Bongrand C, Ruby EG. 2019. The impact of *Vibrio fischeri* strain variation on host colonization. Curr Opin Microbiol 50:15–19. https://doi.org/10.1016/j.mib.2019.09.002.
59. Mandel MJ. 2010. Models and approaches to dissect host-symbiont specificity. Trends Microbiol 18:504–511. https://doi.org/10.1016/j.tim.2010.07.005.
60. Wollenberg MS, Ruby EG. 2009. Population structure of *Vibrio fischeri* within the light organs of *Euprymna scolopes* squid from two Oahu (Hawaii) populations. Appl Environ Microbiol 75:193–202. https://doi.org/10.1128/AEM.01792-08.
61. Bongrand C, Ruby EG. 2019. Achieving a multi-strain symbiosis: strain behavior and infection dynamics. ISME J 13:698–706. https://doi.org/10.1038/s41396-018-0305-8.
62. Wollenberg MS, Ruby EG. 2012. Phylogeny and fitness of *Vibrio fischeri* from the light organs of *Euprymna scolopes* in two Oahu, Hawaii populations. ISME J 6:352–362. https://doi.org/10.1038/ismej.2011.92.
63. Rotman ER, Bultman KM, Brooks JF, II, Gyllborg MC, Burgos HL, Wollenberg MS, Mandel MJ. 2019. Natural strain variation reveals diverse biofilm regulation in squid-colonizing *Vibrio fischeri*. J Bacteriol 201:e00033-19. https://doi.org/10.1128/JB.00033-19.
64. Bongrand C, Moriano-Gutierrez S, Arevalo P, McFall-Ngai M, Visick KL, Polz M, Ruby EG. 2020. Using colonization assays and comparative genomics to discover symbiosis behaviors and factors in *Vibrio fischeri*. mBio 11:e03407-19. https://doi.org/10.1128/mBio.03407-19.
65. Pankey MS, Foxall RL, Ster IM, Perry LA, Schuster BM, Donner RA, Coyle M, Cooper VS, Whistler CA. 2017. Host-selected mutations converging on a global regulator drive an adaptive leap towards symbiosis in bacteria. Elife 6:e24414. https://doi.org/10.7554/eLife.24414.
66. Yip ES, Grublesky BT, Hussa EA, Visick KL. 2005. A novel, conserved cluster of genes promotes symbiotic colonization and σ^{54}-dependent biofilm formation by *Vibrio fischeri*. Mol Microbiol 57:1485–1498. https://doi.org/10.1111/j.1365-2958.2005.04784.x.
67. Hunt TP, Magasanik B. 1985. Transcription of *glnA* by purified *Escherichia coli* components: core RNA polymerase and the products of *glnF*, *glnG*, and *glnL*. Proc Natl Acad Sci U S A 82:8453–8457. https://doi.org/10.1073/pnas.82.24.8453.
68. Soutourina OA, Bertin PN. 2003. Regulation cascade of flagellar expression in Gram-negative bacteria. FEMS Microbiol Rev 27:505–523. https://doi.org/10.1016/S0168-6445(03)00064-0.
69. Prouty MG, Correa NE, Klose KE. 2001. The novel σ^{54}- and σ^{28}-dependent flagellar gene transcription hierarchy of *Vibrio cholerae*. Mol Microbiol 39:1595–1609. https://doi.org/10.1046/j.1365-2958.2001.02348.x.
70. McCann J, Stabb EV, Millikan DS, Ruby EG. 2003. Population dynamics of *Vibrio fischeri* during infection of *Euprymna scolopes*. Appl Environ Microbiol 69:5928–5934. https://doi.org/10.1128/aem.69.10.5928-5934.2003.
71. Le Roux F, Binesse J, Saulnier D, Mazel D. 2007. Construction of a *Vibrio splendidus* mutant lacking the metalloprotease gene *vsm* by use of a novel counterselectable suicide vector. Appl Environ Microbiol 73:777–784. https://doi.org/10.1128/AEM.02147-06.
72. Bao Y, Lies DP, Fu H, Roberts GP. 1991. An improved Tn7-based system for the single-copy insertion of cloned genes into chromosomes of gram-negative bacteria. Gene 109:167–168. https://doi.org/10.1016/0378-1119(91)90604-a.
73. Simon R, Priefer U, Pühler A. 1983. A broad host range mobilization system for *in vivo* genetic engineering: transposon mutagenesis in gram negative bacteria. Nat Biotechnol 1:784–791. https://doi.org/10.1038/nbt1183-784.
74. Khodursky AB, Bernstein JA, Peter BJ, Rhodius V, Wendisch VF, Zimmer DP. 2003. *Escherichia coli* spotted double-strand DNA microarrays: RNA extraction, labeling, hybridization, quality control, and data management. Methods Mol Biol 224:61–78. https://doi.org/10.1385/1-59259-364-X:61.
75. Ross W, Sanchez-Vazquez P, Chen AY, Lee J-H, Burgos HL, Gourse RL. 2016. ppGpp binding to a site at the RNAP-DksA interface accounts for its dramatic effects on transcription initiation during the stringent response. Mol Cell 62:811–823. https://doi.org/10.1016/j.molcel.2016.04.029.
76. Livak KJ, Schmittgen TD. 2001. Analysis of relative gene expression data using real-time quantitative PCR and the $2^{-\Delta\Delta C^T}$ method. Methods 25:402–408. https://doi.org/10.1006/meth.2001.1262.
77. Karp PD, Billington R, Caspi R, Fulcher CA, Latendresse M, Kothari A, Keseler IM, Krummenacker M, Midford PE, Ong Q, Ong WK, Paley SM, Subhraveti P. 2019. The BioCyc collection of microbial genomes and metabolic pathways. Brief Bioinform 20:1085–1093. https://doi.org/10.1093/bib/bbx085.
78. Mandel MJ, Stabb EV, Ruby EG. 2008. Comparative genomics-based investigation of resequencing targets in *Vibrio fischeri*: focus on point miscalls and artefactual expansions. BMC Genomics 9:138. https://doi.org/10.1186/1471-2164-9-138.
79. Brooks JF, II, Mandel MJ. 2016. The histidine kinase BinK is a negative regulator of biofilm formation and squid colonization. J Bacteriol 198:2596–2607. https://doi.org/10.1128/JB.00037-16.
80. Boettcher KJ, Ruby EG. 1990. Depressed light emission by symbiotic *Vibrio fischeri* of the sepiolid squid *Euprymna scolopes*. J Bacteriol 172:3701–3706. https://doi.org/10.1128/jb.172.7.3701-3706.1990.